

Characterizing the Effect of Altering the Floor of a Laboratory Water Tank on Hydroacoustic
Signals

Sarianne Winters

Physics 492R Capstone Project Report

04/17/2025

Advisor: Dr. Traci Neilsen

Abstract

Sound signals in the ocean can be affected by changes in seabed material properties. The goal of this project is to conduct preliminary studies to investigate the amount of change we would expect in the spectral properties of a received signal by introducing small changes in the bottom of a laboratory water tank. In this project, different materials were tested by placing them at the bottom of the laboratory tank and sending an acoustic signal between source and receiver hydrophones in the water. Different frequency bands were tested for each material using a linear chirp as the signal. The results of a transfer function analysis showed that altering the tank floor material causes small frequency-dependent changes in the received signal. These changes can be representative of similar changes that may occur in the ocean due to varying seabed material.

Introduction

As sound waves propagate through the ocean, several wave phenomena affect their propagation, including refraction, reflection, and scattering. Refraction originates from changes in sound speed; reflections occur at interfaces where the impedance changes suddenly; and scattering may occur when sound hits an uneven surface, causing the sound wave to scatter in different directions. It is important in acoustical research and underwater technology to understand how changes in the seafloor reflectivity and roughness affect the way sound signals propagate.

Considerable research has been done on how seafloor properties and roughness are linked to the seabed reflection coefficient. Measurements of seabed reflectivity can help characterize the density and thickness of different layers in the seafloor (Holland, 2004; Dosso, 2005; Dettmer,

2007; Dettmer 2009; Belcourt, 2019; Holland, 2021). Conversely, for known seabed properties, the reflectivity can be calculated using numerical models. Recent work (Holland, 2017; Olson, 2023) gives an estimate for calculating the seabed reflection coefficient and highlights the effect of scattering due to seafloor roughness. These studies highlight how an understanding of seabed reflectivity is essential for modeling underwater sound propagation.

This project contributes to this topic by characterizing the effect that different “seafloor” materials have on the propagation of acoustic signals in a controlled laboratory setting. This approach has allowed for investigating several different tank floor materials while keeping other variables controlled. The results of this project are most applicable to our laboratory water tank and other similar tanks, but the results can also contribute to the discussion on seafloor variations.

Methods

Using a laboratory water tank for acoustical measurements allows for greater control over variables. Water temperature, surface conditions, and seafloor properties are more difficult to identify in an ocean environment than in a laboratory tank. In order to ensure that any changes in the tank measurements were caused by the changes in the floor material, all other variables must be kept constant.

To allow for greater control over independent variables, the measurements for this project were taken in a laboratory water tank, as shown in Figure 1. The tank used for this project is an open-air acrylic tank located in the Hydroacoustics lab at BYU. This tank has a 48 square foot base and a maximum depth of 0.9 meters. The water level was kept at a depth of 0.6 meters for

all of the measurements taken in this project. The tank walls are lined with echo reduction panels to minimize reflections off the sides of the tank.

The tank is equipped with robots to hold the source and receiver hydrophones. For this project B&K 8103 transducers are used as both the transmitter and the receiving hydrophone. These transducers are attached to the robots that can move them to specified positions in the water tank. The robots are controlled through a custom LabView program called ESAU (Easy Spectrum Acoustics Underwater). ESAU also controls the signal generation and data acquisition through the hydrophones.

ESAU was also used to generate the signals. For these measurements, one second long linear chirps (with amplitudes of 1000 mV) over different frequency bands were generated by ESAU, were converted to analog by a Spectrum D/A card, and passed through the TEGAM power amplifier before being sent to the transmitter. The signal propagated through the tank and the signal received by the hydrophone was passed through the NEXXUS signal conditioner box, converted to a digital signal using a Spectrum A/D card, and saved by ESAU in a binary format. Additional details about the measurement chain are provided in Vongsawad (2021).

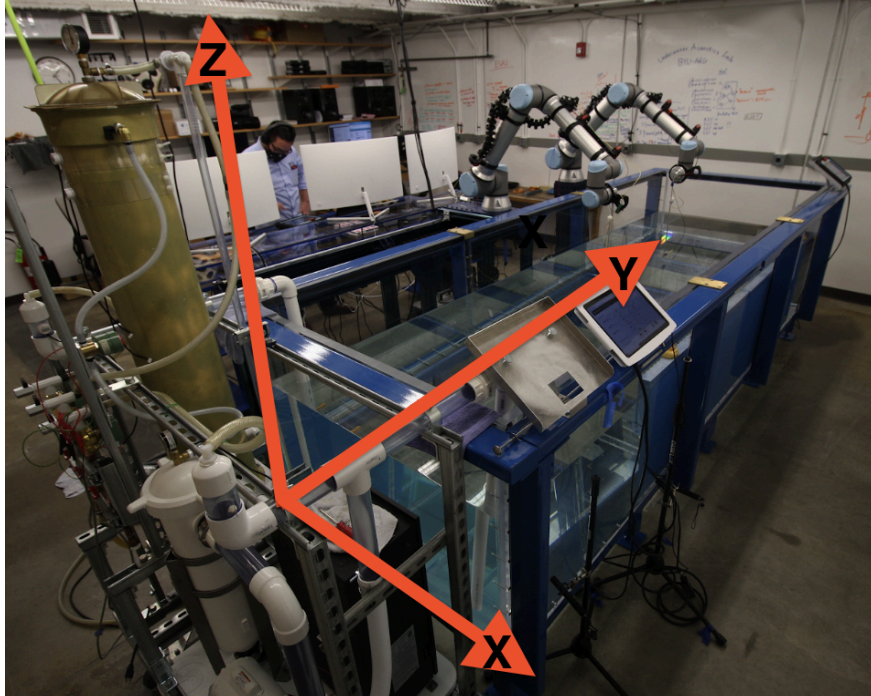


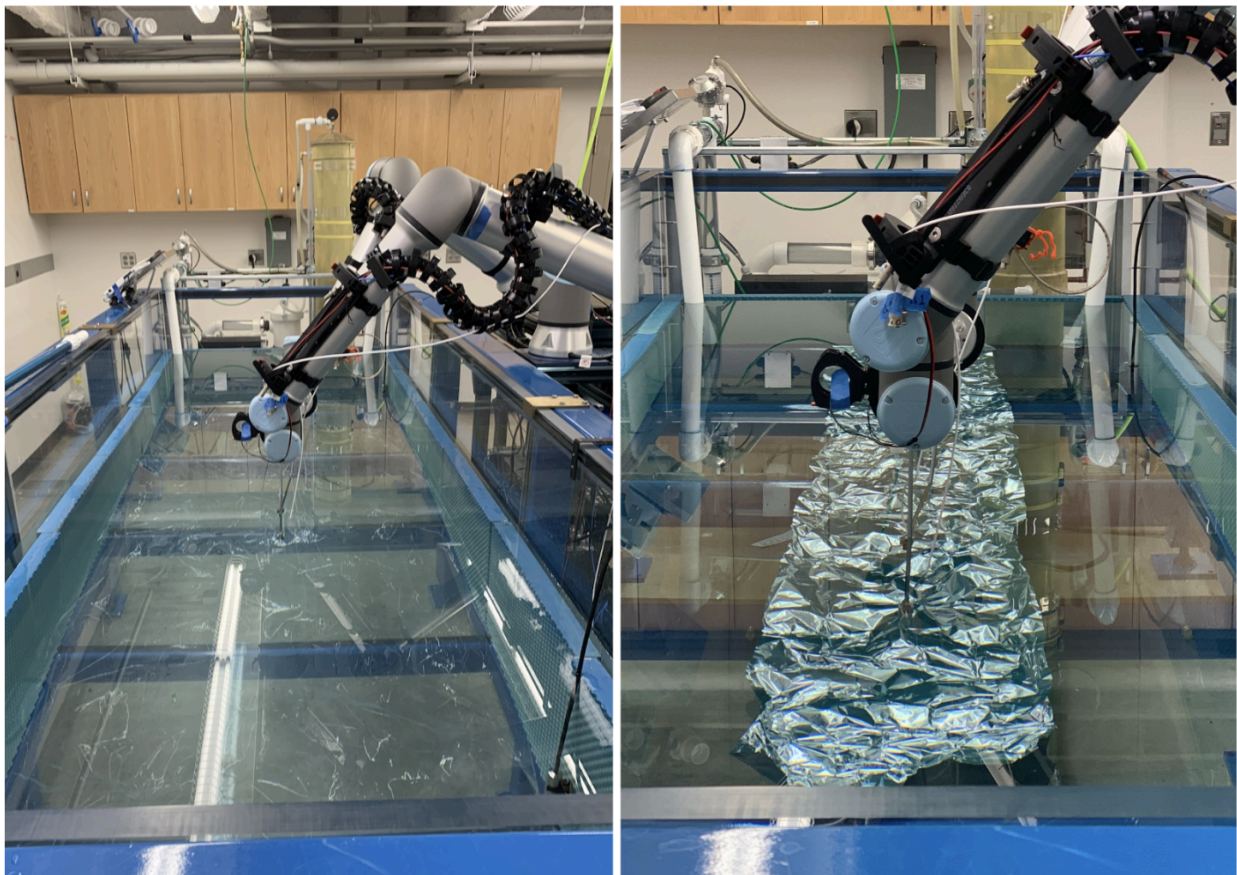
Figure 1: Acrylic water tank in the BYU hydroacoustics lab. Arrows show the direction of the x , y , and z axes used by the robots. The $(0,0,0)$ location is the bottom left corner in the above figure, with $+y$ extending towards the far wall, $+x$ extending towards the right side of the tank, and $+z$ extending up from the base of the tank.

For this project, measurements were taken with different materials on the tank floor underneath the transducers and with chirps covering different frequency bands. Table 1 outlines the conditions of each scan. There were four measurement scans taken on day 1: two with the acrylic floor and two with the PVC sheet on the tank base. The numbers 1 and 2 in the name column indicate a different tank floor material. The letters A and B indicate a different frequency band. On day 1, there were only two frequency bands used for each floor material, but on days 2 and 3 three frequency bands were used for each material. When acrylic is used to describe the floor material, that simply means that there was no additional material put on top of the tank base. Acrylic just means the regular tank base, because the tank is made of acrylic.

*Table 1: Measurement scans organized according to floor material and frequency band. The * indicates that the PVC sheet was underneath this material. Data are stored on our underwater shares drive: underwater/uw-measurements/2025/*

Name	Date	“Day”	Scan Number	Floor Material	Frequency Band (kHz)
1A	2025-02-12	1	0	acrylic	10-50
1B	2/12	1	1	acrylic	50-100
2A	2/12	1	2	PVC sheet	10-50
2B	2/12	1	3	PVC sheet	50-100
3A	2/26	2	0	acrylic	1-10
3B	2/26	2	1	acrylic	10-50
3C	2/26	2	2	acrylic	50-100
4A	2/26	2	3	aluminum foil	1-10
4B	2/26	2	4	aluminum foil	10-50
4C	2/26	2	5	aluminum foil	50-100
5A	3/12	3	3	aluminum plate*	1-10
5B	3/12	3	4	aluminum plate*	10-50
5C	3/12	3	5	aluminum plate*	50-100
6A	3/12	3	6	rubber block*	1-10
6B	3/12	3	7	rubber block*	10-50
6C	3/12	3	8	rubber block*	50-100
7A	3/12	3	10	acrylic with PVC sheet	1-10
7B	3/12	3	11	acrylic with PVC sheet	10-50
7C	3/12	3	12	acrylic with PVC sheet	50-100

Each day has control scans with the regular acrylic base and then scans with a different material placed on top of the tank base to act as the new tank floor. On day 1, that material was a PVC sheet that covered the entire base of the tank (scans 2A and 2B). On day 2, the material was a strip of aluminum foil (scans 4A, 4B, and 4C). The aluminum foil did not cover the entire base of the tank, but it was placed directly under the hydrophone path. Figure 2 shows the set up of the tank for scans 2A, 2B, 4A, 4B, and 4C.

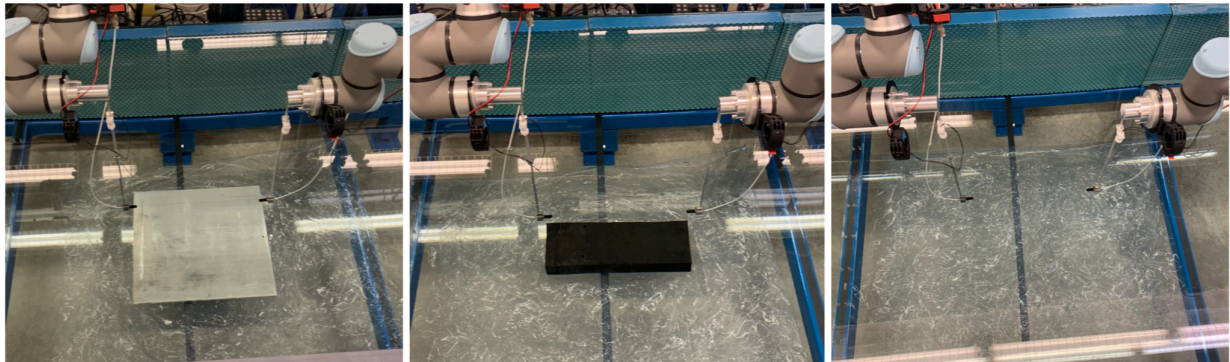


(a) PVC tank floor

(b) Aluminum foil tank floor

Figure 2: (a) PVC sheet lining the bottom of the tank. (b) Strip of aluminum foil on the bottom of the tank underneath the hydrophone path.

On day 3, there were 2 different materials being tested in addition to the control scan. The materials were an aluminum plate with dimensions 17.75 x 16 x 0.5 inches and a rubber block with dimensions: 17 x 5.5 x 3 inches. In order to protect the tank from possible scratching due to the sharp edges of these materials, these items were not placed directly on the tank base. Rather, the PVC sheet was used as a protective layer between the acrylic tank base and the other material (either the aluminum plate or the rubber block). Because of this, the control scans for day 3 were taken with the PVC sheet on top of the tank base (scans 7A, 7B, and 7C). This allows for better analysis of the effects of just the material of interest, instead of the combined effects of the material and the protective PVC layer. Figure 3 shows the set up of the tank for the scans taken on day 3.



(a) Aluminum plate

(b) Rubber block

(c) PVC sheet

Figure 3: (a) Aluminum plate as the tank floor with PVC sheet underneath it to protect the acrylic tank base. (b) Rubber block as the tank floor with PVC sheet underneath it to protect the acrylic tank base. (c) PVC sheet without any additional material as a control scan.

Both the source and receiver hydrophones were positioned in the center of the tank depth wise (z direction) and width wise (x direction). The x direction corresponds to the width of the

tank which is the shorter end of the tank, the y direction goes along the longer length of the tank, and the z direction goes up and down, so it corresponds to the depth of the tank (see figure 1). While the x and z positions (of 60 cm and 31 cm, respectively) remained the same for both hydrophones, the y position of the receiver hydrophone was varied during each scan on days 1 and 2 to change the distance between the hydrophones. Each scan on these first 2 days had 51 different hydrophone distances ranging from 0.15 - 1.65 m. For each of these distances in a single scan, the same acoustic signal was sent from the source hydrophone; a linear chirp sweeping through the range of frequencies as specified in Table 1. Because of the size of the materials tested on day 3, it was not feasible to test a wide range of y-distances. Hence the y-position of the receiver hydrophone remained constant for these scans. The y-position was chosen to be 30 cm so that the base of the tank directly underneath and between the hydrophones was covered by the material.

This report focuses on the results when the hydrophone distance was kept constant in all directions. The data in the results section is only looking at the chirps from days 1 and 2 that correspond to the same y-distance of 30 cm between the hydrophones that was used on day 3.

In order to analyze the data from each of these scans, a Jupyter notebook running Python code was used.¹ This code reads in the data file from ESAU and can graph the waveform and power spectral density (PSD) via the Welch method. It can also plot the spectra for multiple scans in the same plot for comparison.

¹ Path to code: `underwater/sarianne-winters/code/uw-measurements/new_spectral_analysis_bin.ipynb`

To perform the Fourier transform, the Welch method is used via the `scipy.signals.welch` function. This function divides the signal into blocks with overlap, applies a windowing function, calculates the Fourier transform of each block, and converts to single-sided spectral density levels: $X_i(f)$, where i indicates which block. The spectral density for the different time blocks are stacked into a matrix $\mathbf{X} = [X_1(f), X_2(f), \dots, X_{nt}(f)]$, where nt is the total number of blocks. A time-averaged over the blocks yields the power spectral density: $\text{PSD} = \mathbf{X}^* \mathbf{X}$, where $*$ indicates the complex conjugate. The power spectral density levels are computed as $10 \cdot \log_{10}(\text{PSD}/\text{pref}^2)$.

Another useful quantity for computing is the cross spectral density: CSD. This is useful for comparing two signals $x(t)$ and $y(t)$. In the notation used above, the Welch method is used to calculate the spectral density over time blocks for each signal: $\mathbf{X} = [X_1(f), X_2(f), \dots, X_{nt}(f)]$ and $\mathbf{Y} = [Y_1(f), Y_2(f), \dots, Y_{nt}(f)]$. The cross spectral density is $\text{CSD} = \mathbf{X}^* \mathbf{Y}$. The CSD is used for calculating transfer functions in the results section.

Results and Discussion

Each graph in Figure 4 and Figure 5 shows two scans plotted together on the same graph. The blue line is the control scan. This is the acrylic tank base for the top two graphs of each figure, which corresponds to scans 1A and 3B for Figure 4, and scans 1B and 3C for Figure 5. The control scans for the bottom two graphs of each figure is the acrylic tank base with the protective PVC layer. For Figure 4 this is scan 7B, and for Figure 5 it is scan 7C. The orange line of each graph in Figures 4 and 5 is the PSD of the scans with a different material added on top of the control. The title of each graph indicates this material. Figure 4 shows PSD graphs of each

material with a 10-50 kHz frequency band, and Figure 5 shows the graphs with a 50-100 kHz frequency band.

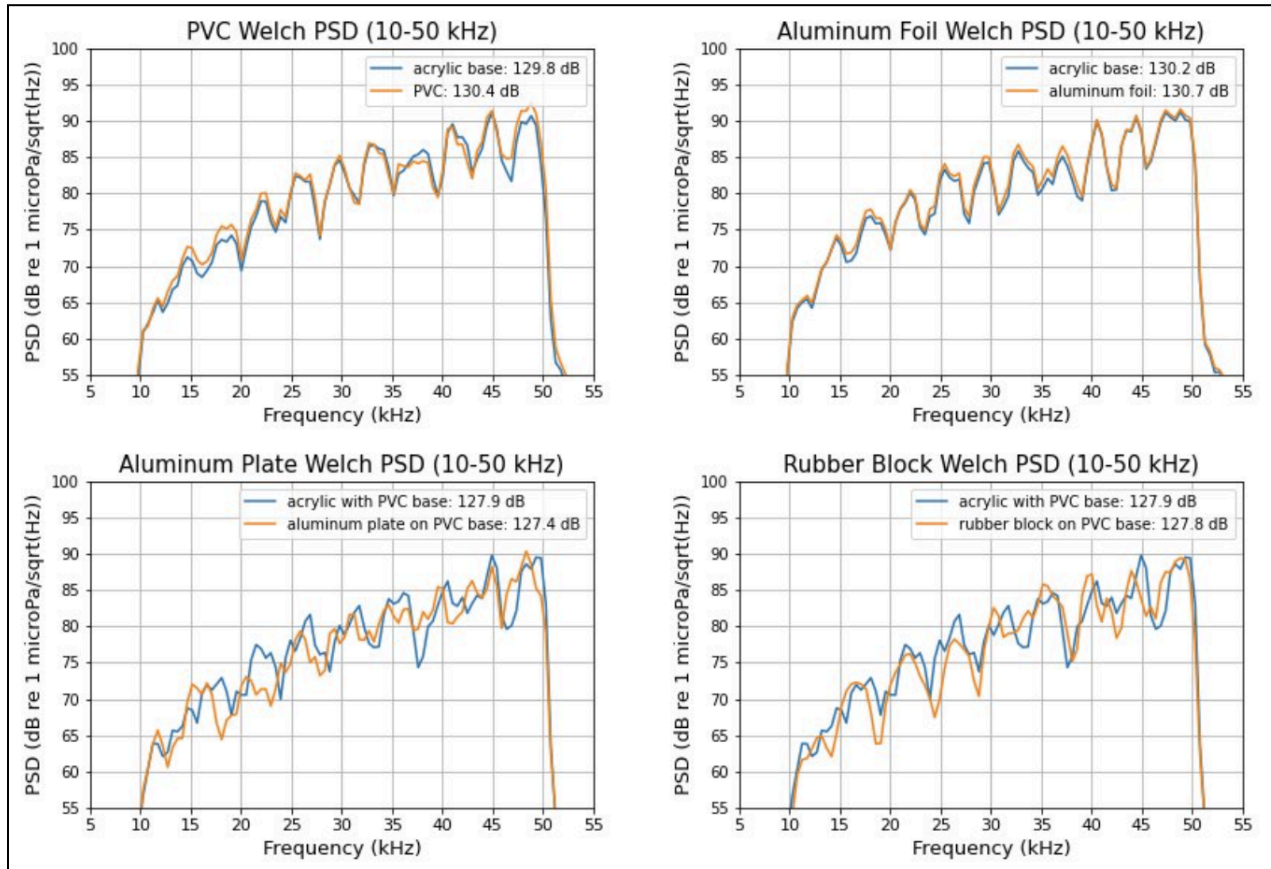


Figure 4: Power spectral density graphs via Welch method for each tank floor material (compared to the control tank base) with a 10-50 kHz frequency band.

The code also calculates the overall sound pressure level (OASPL) received for each scan. The OASPL in decibels (dB re 1 microPa/sqrt(Hz)) for each scan is displayed on the legend of each graph in Figures 4 and 5. For each of these graphs, the difference between the OASPL of the changed material scan and the corresponding control scan is always less than 0.7 dB. This can be considered a very small difference because the sound pressure levels are over 120 dB for every scan. In addition to this seemingly negligible difference in the OASPL levels,

there is also not much variation in the shape of the PSD graphs (The blue and orange lines look very similar in each graph, and are almost identical in the PVC scans and the aluminum foil scans.)

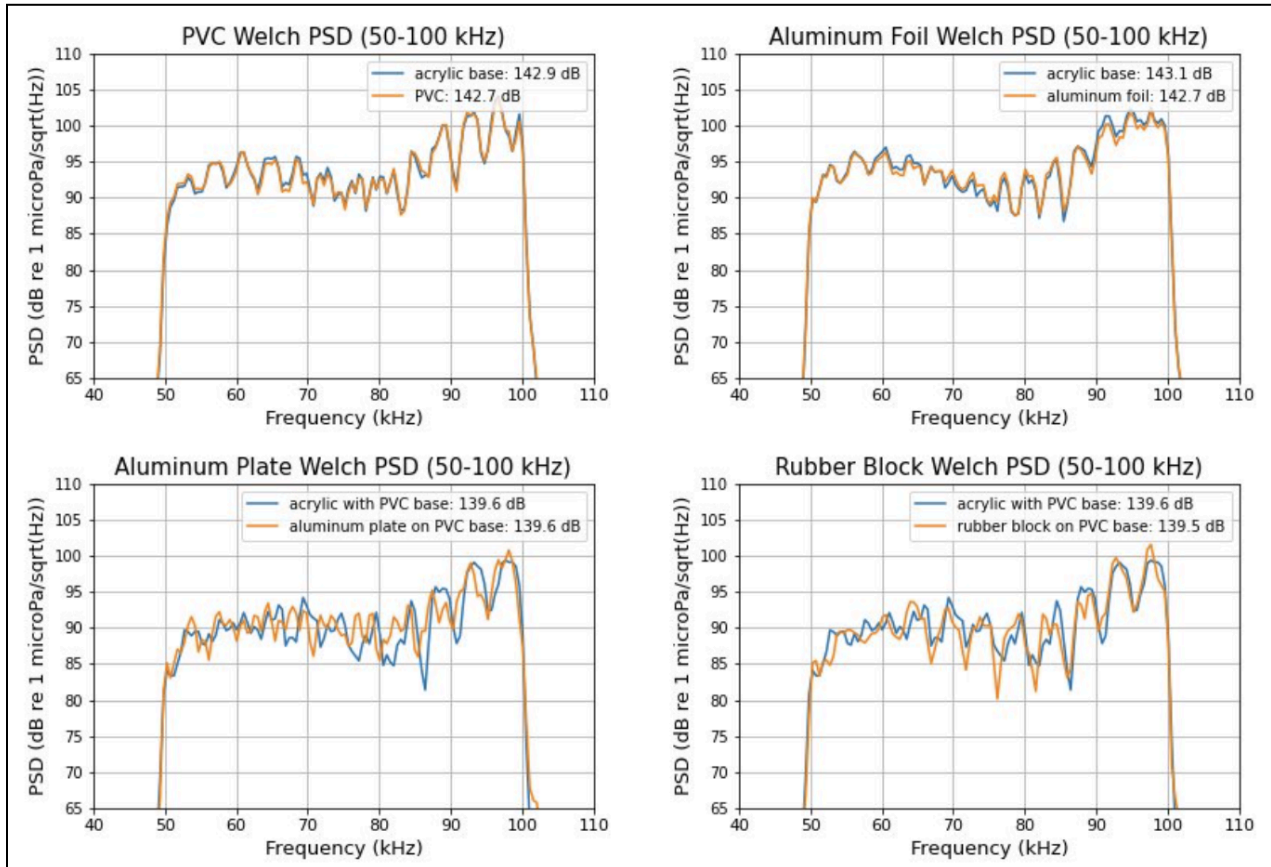


Figure 5: Power spectral density graphs via Welch method for each tank floor material (compared to the control tank base) with a 50-100 kHz frequency band.

At first glance, this makes it seem like changing the tank floor material did not significantly impact the path or strength of the acoustic signal. However, it is likely that these results are so similar because most of the paths that the sound travels in remain unchanged throughout the different scans. Much of the sound signal travels in a direct path through the water from the source hydrophone to the receiver. Some of the signal reflects off of the surface

of the water, which also does not change between scans. The only thing that is changing is the material on the base of the tank, which only has an effect on a limited number of the possible paths the sound could take from the source to the receiver. So it makes sense that the OASPL and PSD spectra do not show a significant change in the total sound signal received.

In order to see the effects of changing the base of the tank, the part of the acoustic signal that is impacted by the tank floor needs to be isolated. Most of the signal is not impacted by the floor, but there are parts of the signal that reflect off of the bottom of the tank. This is the part of the signal that is of most interest for this project. One way to look at the difference between two functions is to use a transfer function. In our tank, the transfer function tells us how the sound was modified as it traveled.

The received signal $r(t)$ is the convolution of the source signal $s(t)$ and the impulse response $h(t)$ of the tank environment that it travels through; $r(t) = s(t)*h(t)$. The impulse response should be changed by the addition of materials on the tank base. When a Fourier transform is applied to the received signal, the convolution between the source signal and the impulse response is changed to the product of the source spectrum $S(f)$ and the transfer function $H(f)$ where $S(f) = \text{FFT}(s(t))$ and $H(f) = \text{FFT}(h(t))$. Thus the spectrum of the received signal is $R(f) = \text{FFT}(r(t)) = S(f)H(f)$. (In our case, the source spectrum $S(f)$ is known because it is the monitor signal.) In general, the transfer function can be obtained by dividing the spectrum of the received signal by the source spectrum; $H(f) = R(f)/S(f)$. The transfer function $H(f)$ shows how the propagation impacted the signal going from the source to the receiver.

In this work, however, the quantity of interest is how the transfer function changes when a different material is added to the bottom of the tank. Because the source spectrum $S(f)$ is the same in the two cases, the ratio of the received spectra yields the ratio of the transfer functions: $R_2/R_1 = H_2/H_1 = H_{21}$. This ratio is calculated for each frequency, and $H_{21}(f)$ contains the frequency dependent differences between the transfer function with the two different bottom conditions; i.e., everything that is the same between the two signals has been removed. For stability, the transfer function H_{21}^* is calculated with the cross spectrum between spectral density R_1 from the base measurement and spectral density R_2 from the measurement with the different material. The specific equation is $H_{21} = R_1^* R_2 / R_1 R_1^*$. Plots of H_{21} are shown in Figures 6 and 7 quantify the change in the signal due to a difference in tank floor material.

Figure 6 shows three transfer function graphs on a logarithmic scale. The three different graphs correspond to three different frequency bands (1-10, 10-50, and 50-100 kHz) as shown on the x-axis. This figure only uses the scans from day 3. The blue line is the transfer function (relative to the base measurement) with the aluminum plate, and the orange line is for the rubber block. Figure 7 shows the same transfer functions, but with the y-axis adjusted to a logarithmic scale. The transfer function H_{21} is essentially showing the difference between the measurements for the scan with the changed material (the aluminum plate for the blue line and the rubber block for the orange line) and the control scan, which is the acrylic base with the protective PVC layer. When the function in Figure 7 has a y-value of 0, that corresponds to H_{21} being equal to 1, meaning that the signals are the same for the changed material scan and the control scan.

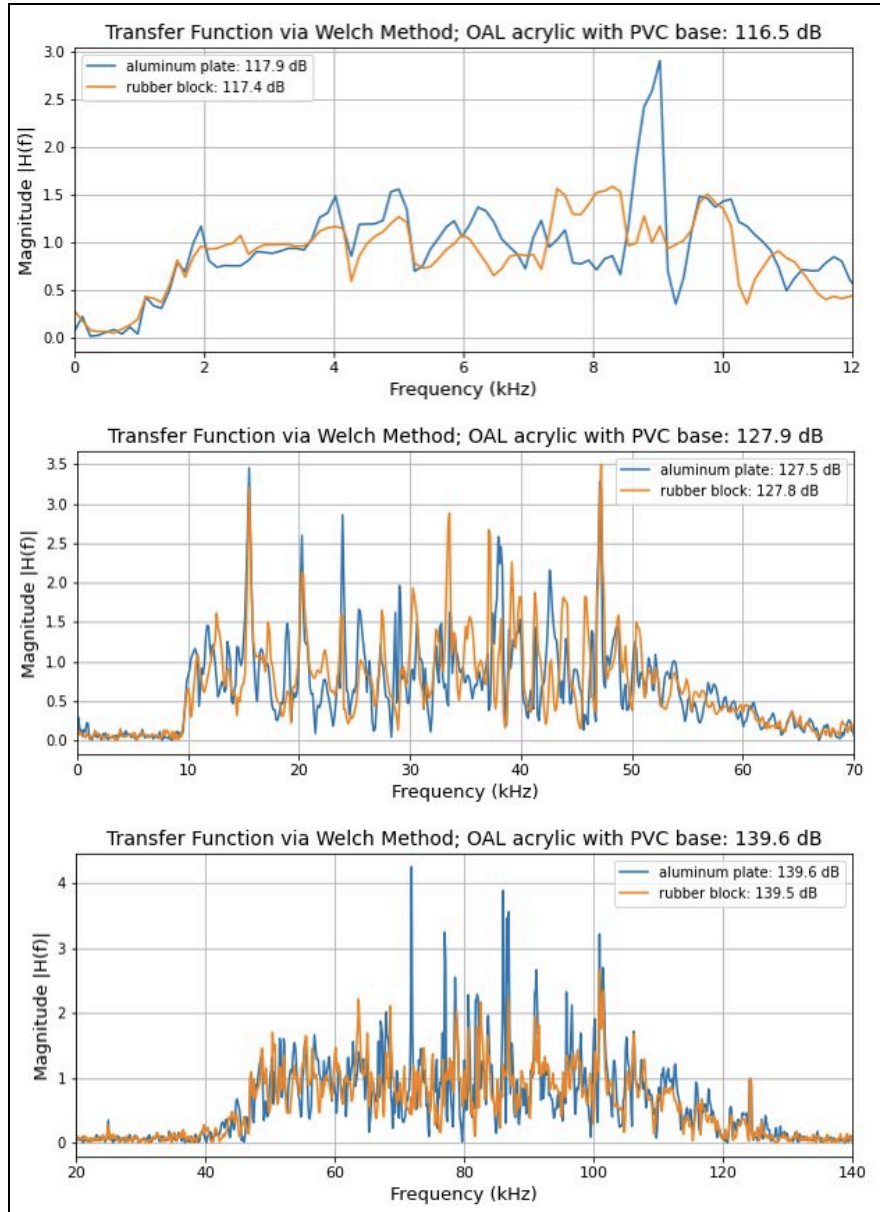


Figure 6: Transfer function magnitude graphs via Welch method for the aluminum plate and the rubber block at 3 different frequency bands.

Concluding Summary

This project was a preliminary study to investigate the amount of change we may expect in the spectral properties of the received signals when introducing small changes in the bottom of the tank. For both the aluminum plate and the rubber block in the 1-10kHz frequency range, differences in the ± 2 dB range were common, and difference was sometimes up to 4 dB. Each material had a slightly different frequency where these larger 4 dB differences occurred. For both higher frequency bands (10-50 kHz and 50-100 kHz), differences of ± 5 dB was common with outliers larger than 10 dB. Using these kinds of materials, we can create frequency-dependent changes that can be representative to changes in ocean seabed.

Several ideas come to mind to further this study. First, the measurements can be redone with larger pieces of the rubber and the aluminum. This approach would allow the comparison of H_{21} as a function of source-receiver distance. In future work, the values of H_{21} need to be compared to the inherent uncertainty in reflectivity measurements as described in Holland (2023). Once these factors are understood, then work may proceed with using tank measurements in deep learning applications for tank floor properties.

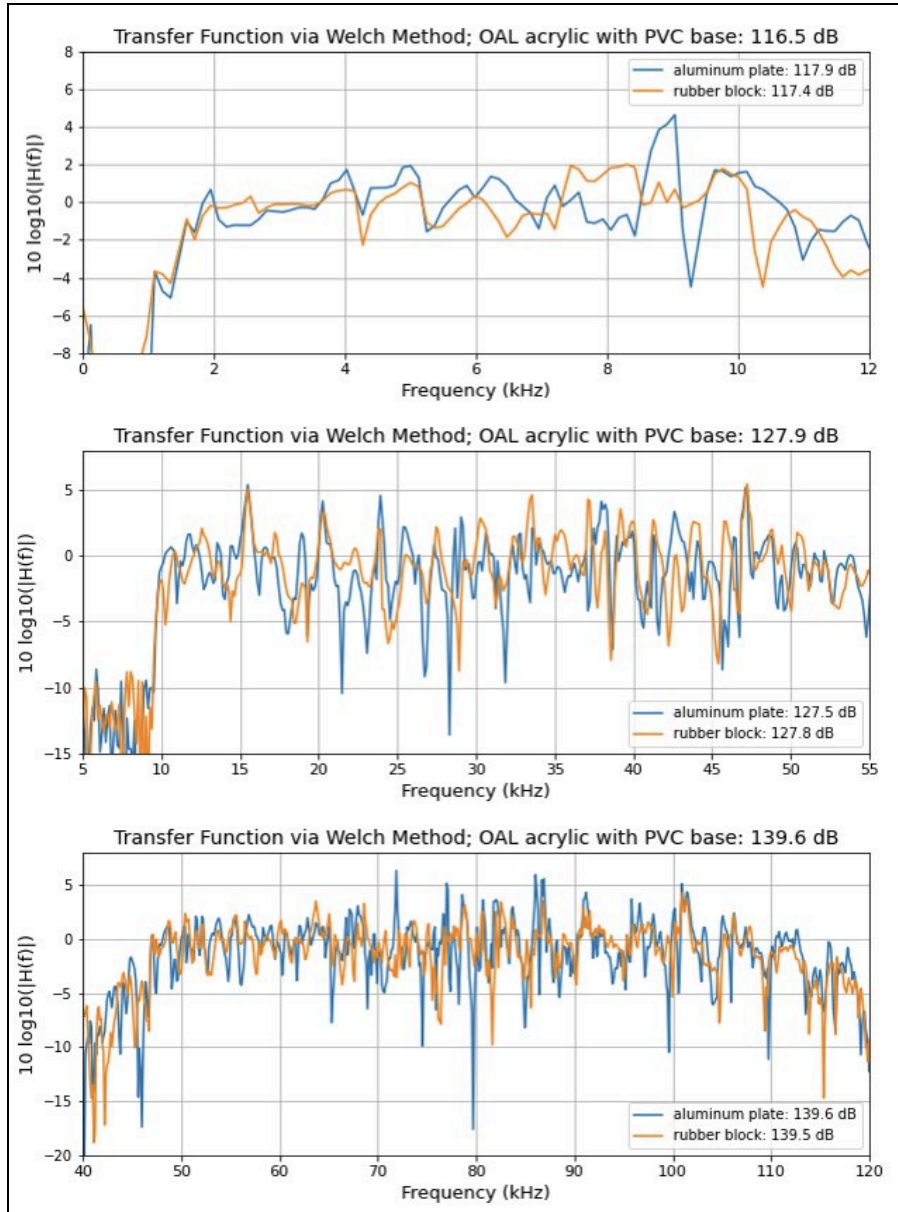


Figure 7: Transfer function graphs via Welch method for the aluminum plate and the rubber block at 3 different frequency bands with the y-axis in dB units.

References

Olson DR. The effect of seafloor roughness on passive estimates of the seabed reflection coefficient. *J Acoust Soc Am*. 2023 Jan;153(1):586. doi: 10.1121/10.0016846. PMID: 36732242.

Belcourt, J., Holland, C. W., Dosso, S. E., Dettmer, J., & Goff, J. A. (2019). Depth-dependent geoaoustic inferences with dispersion at the New England Mud Patch via reflection coefficient inversion. *IEEE Journal of Oceanic Engineering*, 45(1), 69-91.

Dettmer, J., Dosso, S. E., & Holland, C. W. (2007). Full wave-field reflection coefficient inversion. *The Journal of the Acoustical Society of America*, 122(6), 3327-3337.

Dettmer, J., Holland, C. W., & Dosso, S. E. (2009). Analyzing lateral seabed variability with Bayesian inference of seabed reflection data. *The Journal of the Acoustical Society of America*, 126(1), 56-69.

Dosso, S. E., & Holland, C. W. (2006). Bayesian inversion of seabed reflection data. In *Acoustic Sensing Techniques for the Shallow Water Environment: Inversion Methods and Experiments* (pp. 17-27). Dordrecht: Springer Netherlands.

Holland, C. W. (2003). Seabed reflection measurement uncertainty. *The Journal of the Acoustical Society of America*, 114(4), 1861-1873.

HOLLAND, C. W., & HARRISON, C. H. (2004). Measurement of the seabed reflection coefficient in shallow water: A comparison of two techniques. In *Theoretical and Computational Acoustics 2003* (pp. 178-191).

Holland, C. W., Dettmer, J., & Dosso, S. E. (2005). Remote sensing of sediment density and velocity gradients in the transition layer. *The Journal of the Acoustical Society of America*, 118(1), 163-177.

Holland, C. W., Pinson, S., Smith, C. M., Hines, P. C., Olson, D. R., Dosso, S. E., & Dettmer, J. (2017). Seabed structure inferences from TREX13 reflection measurements. *IEEE Journal of Oceanic Engineering*, 42(2), 268-288.

Holland, C. W., Smith, C. M., Lowe, Z., & Dorminy, J. (2021). Seabed observations at the New England Mud Patch: Reflection and scattering measurements and direct geoacoustic information. *IEEE Journal of Oceanic Engineering*, 47(3), 578-593.

Jiang, Y. M., Holland, C. W., Dosso, S. E., & Dettmer, J. (2023). Depth and frequency dependence of geoacoustic properties on the New England Mud Patch from reflection coefficient inversion. *The Journal of the Acoustical Society of America*, 154(4), 2383-2397.

Vongsawad, C. T., Neilsen, T. B., Kingsley, A. D., Ellsworth, J. E., Anderson, B. E., Terry, K. N., ... & Fronk, G. H. (2021, November). Design of an underwater acoustics lab. In *Proceedings of Meetings on Acoustics* (Vol. 45, No. 1). AIP Publishing.

Acknowledgements

I would like to thank the College of Computational, Mathematical, and Physical Sciences at Brigham Young University for providing this research opportunity. I would also like to acknowledge my peers in the Hydroacoustics Lab for their training with the lab equipment and encouragement with this project. Finally, I would like to thank my advisor, Dr. Traci Neilsen, for her indispensable assistance and mentoring.